Electronic Supplementary Material (ESI) for RSC Advances.
This journal is © The Royal Society of Chemistry 2015

ELECTRONIC SUPPLEMENTARY INFORMATION

AFM study of asphalt binder "bee" structures: Origin, mechanical fracture, topological evolution, and experimental artifacts.

Albert M. Hung and Elham H. Fini

S.1. Method of strain application

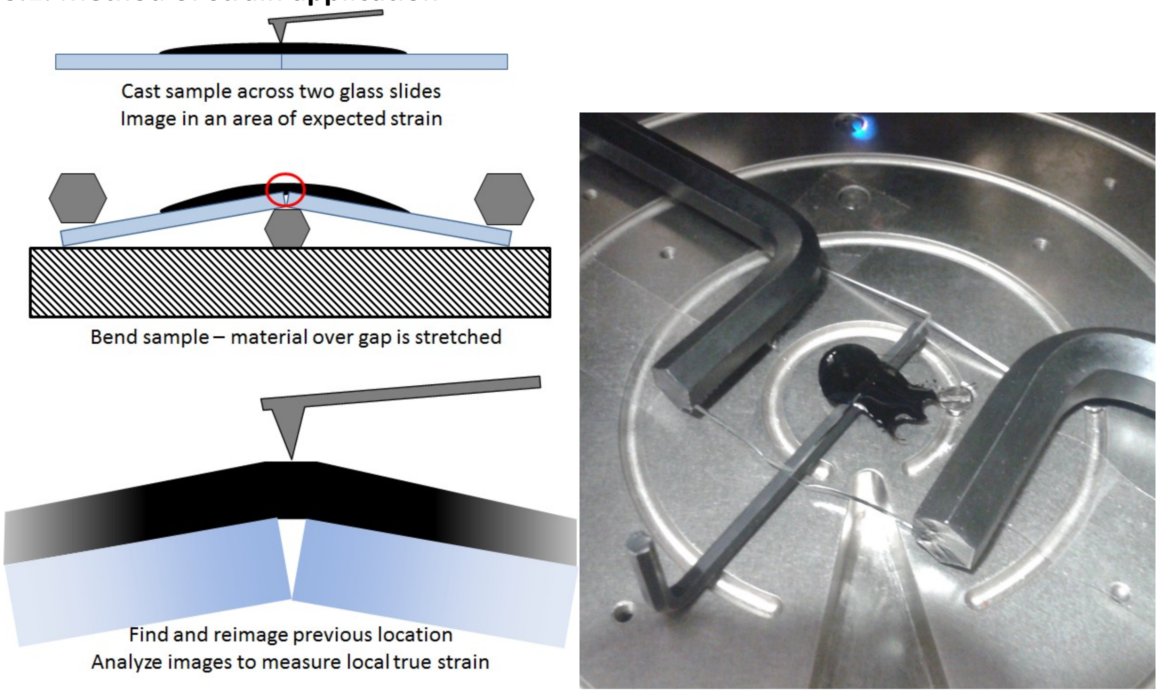

Figure S1. Schematic illustration and photograph of the mechanical strain setup. Bitumen sample is roughly 1 mm thick. Bending is incrementally increased by using progressively larger spacers (hex wrenches). Tape is used to hold the sample together and prevent it from sliding out of position. Shown in the photograph is the sample at maximum deflection with a 4 mm hex wrench. The glass pieces are 37 mm × 25 mm × 1 mm.

S.2. Calculating applied tensile strain from image point displacements

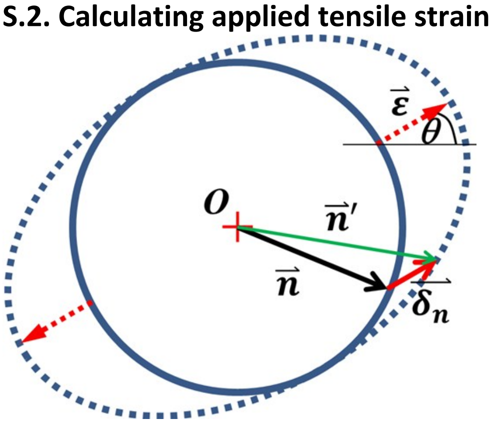

Figure S2. Schematic illustration of vectors used to model displacement of coordinates $\vec{n}$ due to a uniform plane strain $\vec{\varepsilon}$.

The coordinates for a set of 91 points such as asperities and high-contrast spots that could be easily identified in both AFM images taken before and after mechanical stretching were collected. Point coordinates were collected in ImageJ software, and Microsoft Excel was used for simple calculations. The coordinates of a point $\vec{n} = \begin{bmatrix} x \\ y \end{bmatrix}$ in the "before" image is described as a vector from an arbitrary origin $\boldsymbol{O}$ (Figure S2). An applied tensile strain results in a displacement of the coordinates by a vector $\vec{\delta}_n$ so that the new coordinates $\vec{n}'$ are given by:

$$\vec{n}' = \begin{bmatrix} x' \\ y' \end{bmatrix} = \vec{n} + \vec{\delta}_n$$

The deformation is modeled as plane strain (no transverse strain except in the surface normal direction) uniform across the surface and described by a vector $\vec{\varepsilon}$ which can be separated into its magnitude $\boldsymbol{\varepsilon_o}$ and unit vector $\hat{\varepsilon} = \begin{bmatrix} \cos\theta \\ \sin\theta \end{bmatrix}$. The unit vector is described by the orientation angle $\boldsymbol{\theta}$ of the strain relative to the horizontal. In this model, the displacement vector $\vec{\delta}_n$ is given by:

$$\vec{\delta}_n = (\vec{n} \cdot \vec{\varepsilon})\hat{\varepsilon} = \begin{bmatrix} (x\cos\theta + y\sin\theta)\cos\theta \\ (x\cos\theta + y\sin\theta)\sin\theta \end{bmatrix} \varepsilon_o$$

Experimentally, it is impossible to hold the sample perfectly in place, so a second transformation is needed to account for incidental sample rotation by an angle $\boldsymbol{\varphi}$ and sample displacement $\vec{\Delta} = \begin{bmatrix} \Delta_x \\ \Delta_y \end{bmatrix}$. The final predicted coordinates are thus given by $\vec{n}''$:

$$\vec{n}'' = \begin{bmatrix} x'' \\ y'' \end{bmatrix} = \begin{bmatrix} \cos\varphi & -\sin\varphi \\ \sin\varphi & \cos\varphi \end{bmatrix} \vec{n}' + \vec{\Delta} = \begin{bmatrix} (x'\cos\varphi + y'\sin\varphi) + \Delta_x \\ (x'\sin\varphi + y'\cos\varphi) + \Delta_y \end{bmatrix}$$

The predicted coordinates $\vec{n}''$ are compared to the actual coordinates $\vec{n}^*$ collected from the "after" image (deformed sample). The total error $\boldsymbol{E}$ is calculated as the sum of squares of the magnitude of difference between $\vec{n}''$ and $\vec{n}^*$ for all points $\vec{n}$:

$$E = \sum |\vec{n}'' - \vec{n}^*|^2$$

Image displacement $\vec{\Delta}$ was adjusted such that $\sum(\vec{n}'' - \vec{n}^*) = 0$. The transformation parameters $\boldsymbol{\varepsilon_o}$, $\boldsymbol{\theta}$, and $\boldsymbol{\varphi}$ that gave a least squares fit to the "after" coordinates (minimized $\boldsymbol{E}$) are listed in Table S1.

Table S1. Transformation parameters giving a least-squares fit between predicted and real displaced coordinates in AFM images

Tensile strain	ε_o	7.355%
Strain orientation (from horizontal)	θ	24.35°
Sample rotation	φ	0.656°

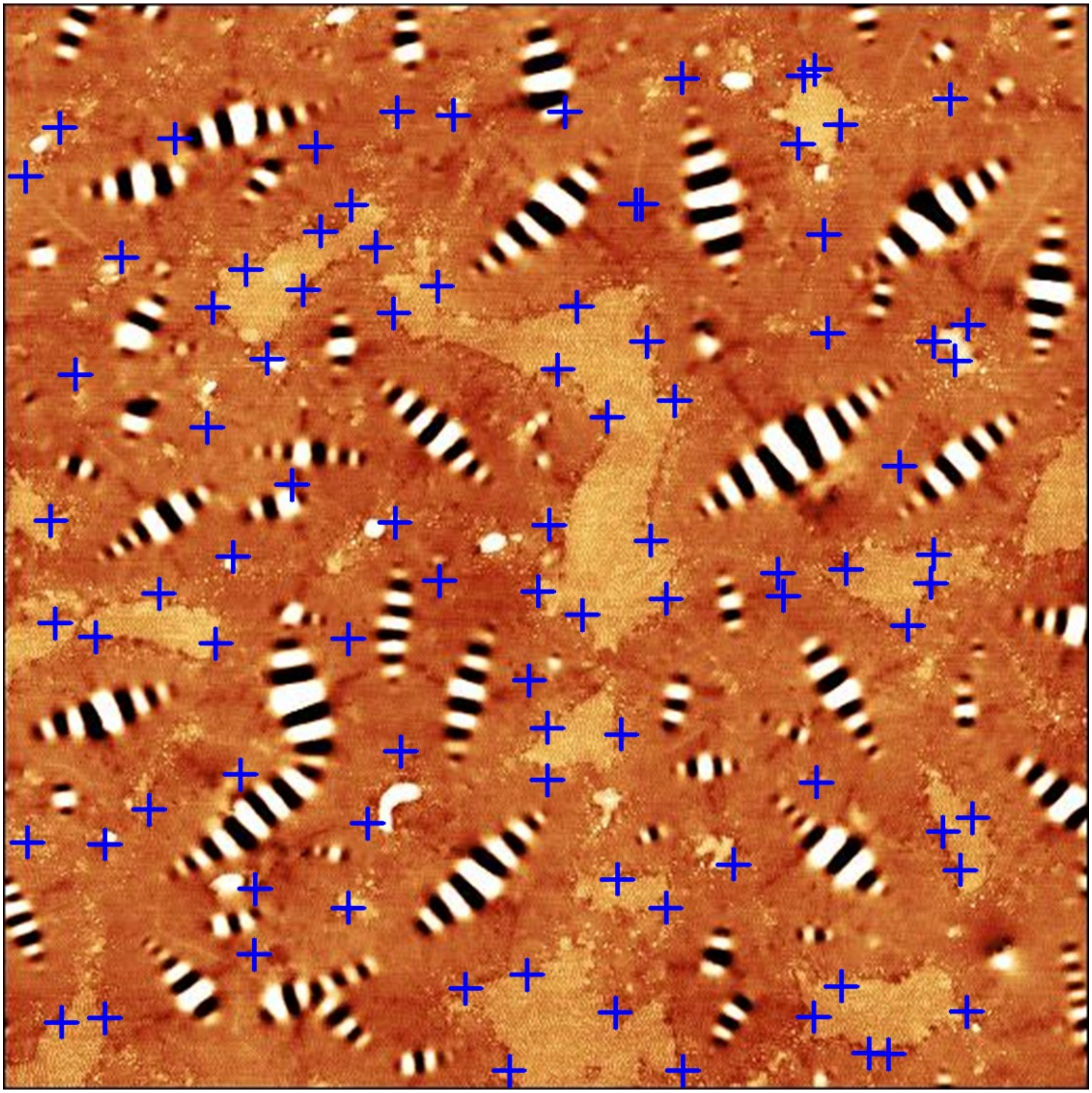

Figure S3a. The AFM images from main text Figures 2a and 2b were flattened and contrasted more severely in order to aid identification of fine features. ImageJ was used to map out 91 points such as asperities and high-contrast spots that could be easily identified in both AFM images taken before and after mechanical stretching.

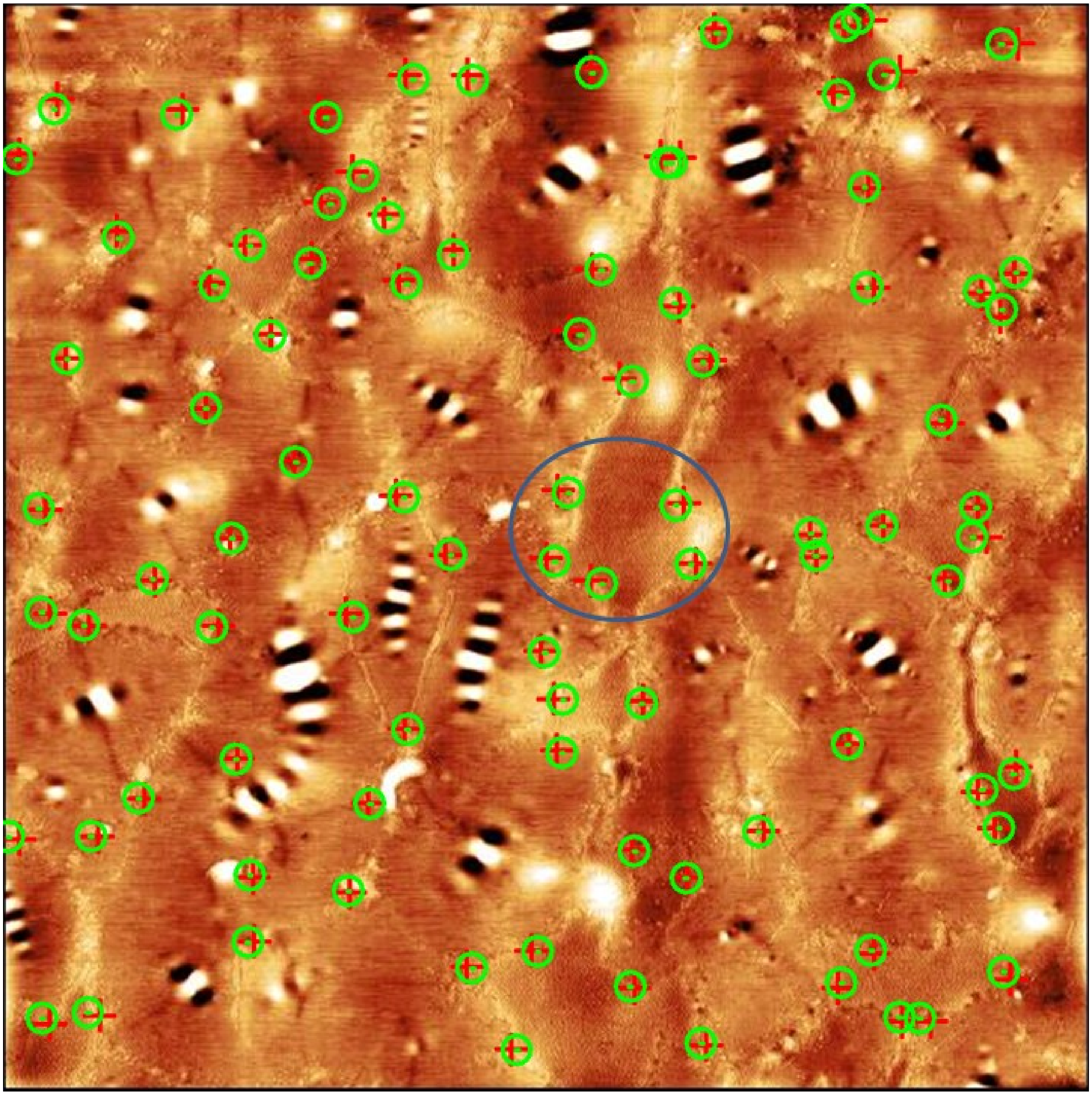

Figure S3b. The points identified in the “before” image (+ in Fig. S3a) are located in the “after” image (+). The “before” coordinates are mathematically transformed to model expected displacement after uniform uniaxial plane strain (O) with corrections for image shift and rotation. Deviations between real and predicted coordinates give further insight into the local distribution of strain. For example, points on the right edge of an interphase area are typically shifted further right of prediction while those on the left edge are shifted left (blue circle). Thus, the para phase area is stretched wider than average, indicating that it is softer than the catana and peri phase.

S.3. Alternate images of strain-fractured “bee” structures

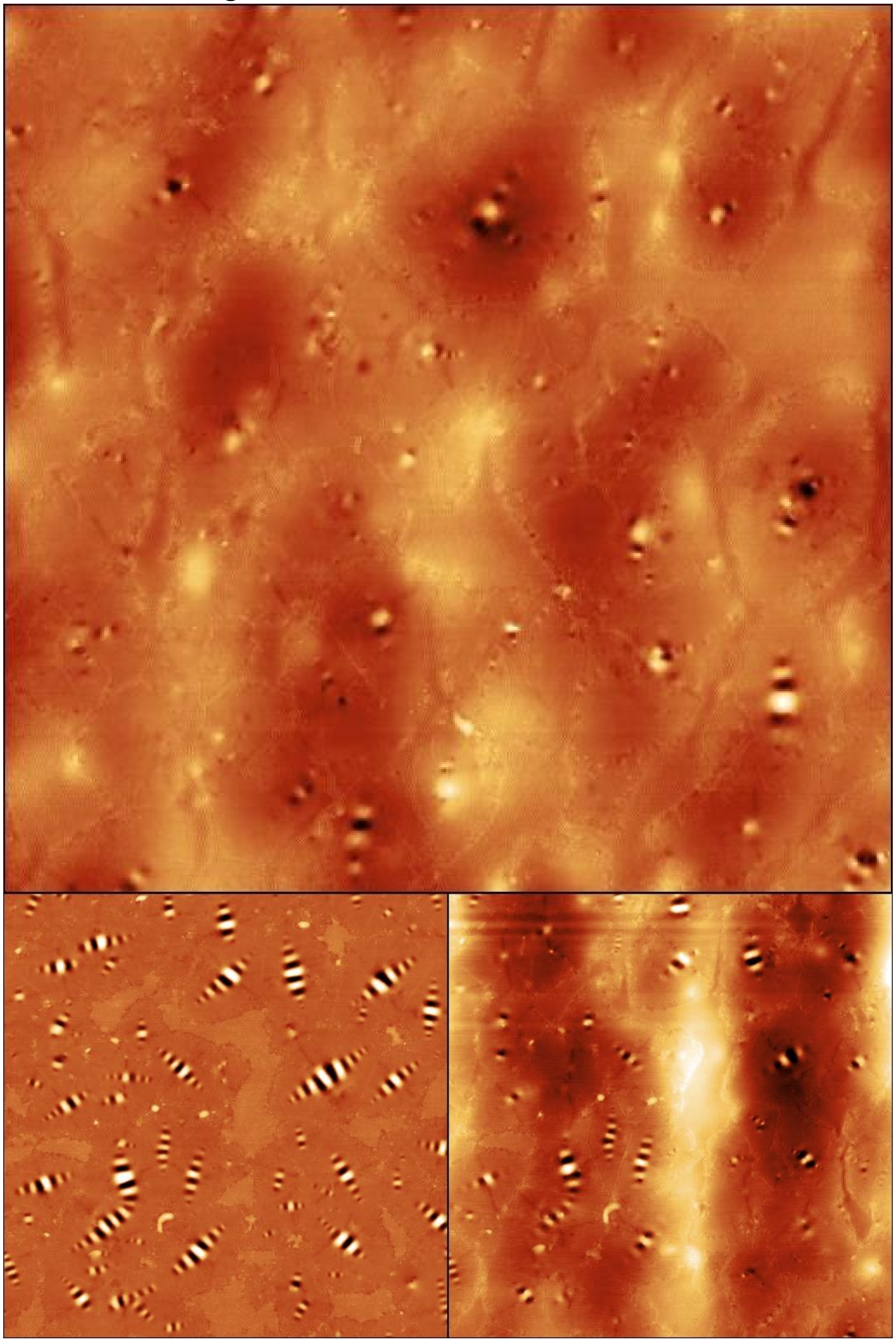

Figure S4. Top: AFM image from main text Fig. 3 with more natural background subtraction (3rd degree polynomial plane fit). Bottom: copies of main text Fig. 2a and 2b for comparison. All scans are 20 μm with 65 nm false color height scale.

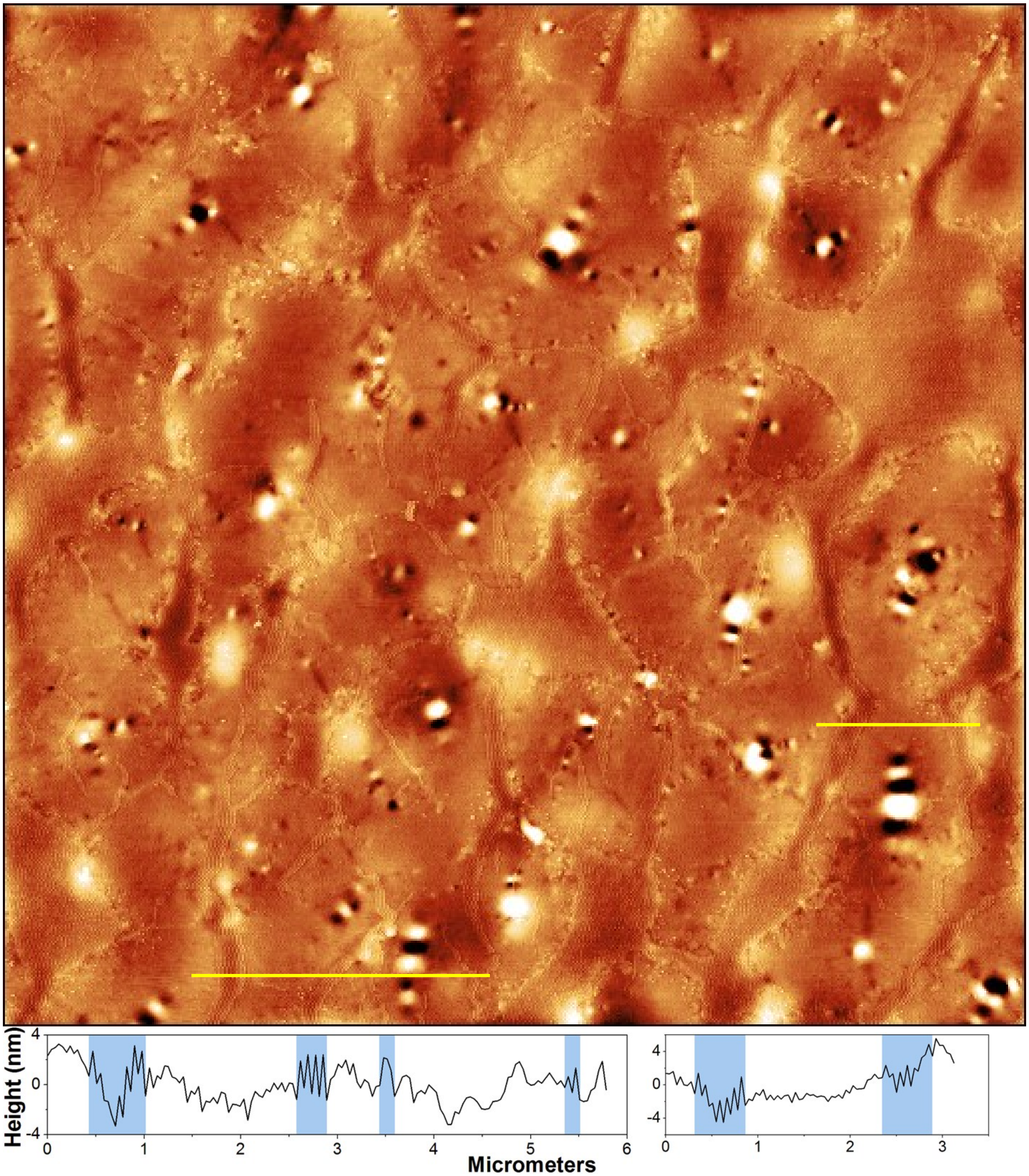

Figure S5. Large version of the same AFM image from main text Fig. 3. The topography image is flattened with 11-degree polynomial background subtraction to aid the identification of fine features. Scan size is 20 μm and false color height scale is 25 nm. Height profile plots of two line traces are shown with blue shading to highlight the location of cracks in or between periphase regions. The cracks appear to be shallow, although shear dilation and tip ringing artifact hinder accurate measurement of the periphase film thickness. The ringing may be a result of stronger tip-sample adhesive forces dampening the cantilever vibration and causing the feedback loop that controls tip lift to overcompensate.

S.4. Additional results: calculation of "bee" wavelengths by fast Fourier transform (FFT) analysis, rheological measurement of PG 64-22, and AFM images of 32 day stored samples

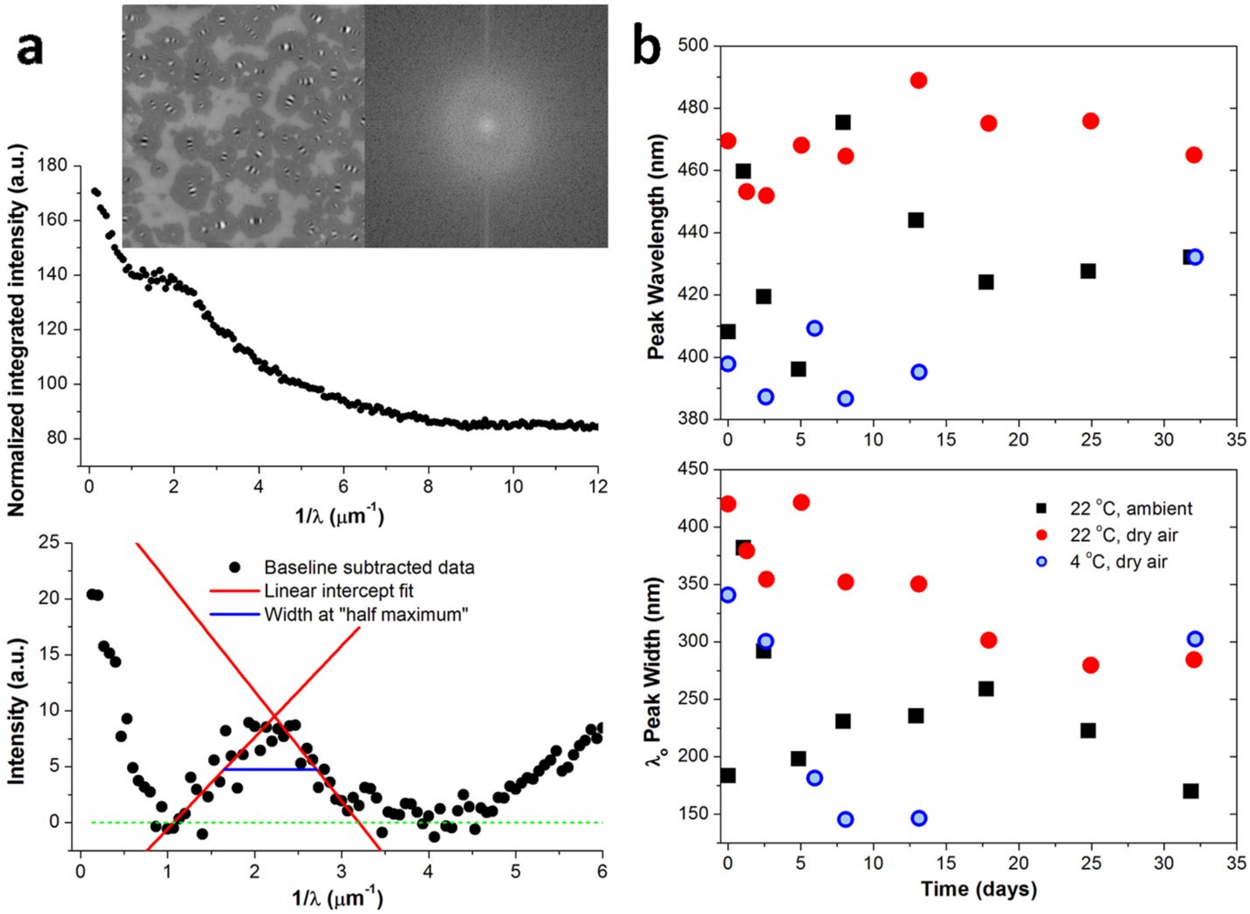

Figure S6. (a) An example of FFT image analysis to determine "bee" wavelength. The FFT of the image (insets) is radially integrated to give an intensity plot showing a peak corresponding to the wavelength of the "bees." Note that the intensity of a point in the FFT plot depends on both amplitude and area of any topological oscillations. A linear baseline is subtracted (green line) and the predominant (mode) wavelength is determined by linear intercept fitting (red lines). Approximating a triangular peak shape, a measure of peak width similar to FWHM can be obtained (blue line). (b) Peak wavelength and width are plotted for bitumen samples under different storage conditions over 32 days. Due to the initial growth conditions, the material may start from an initial state closer to equilibrium. Thus the coarsening effect may be less pronounced than expected, although more data is needed. A decrease in peak width would suggest a narrowing of the wavelength distribution over time that may be due to coarsening or annealing away of kinetically trapped or non-equilibrium wavelengths, for example.

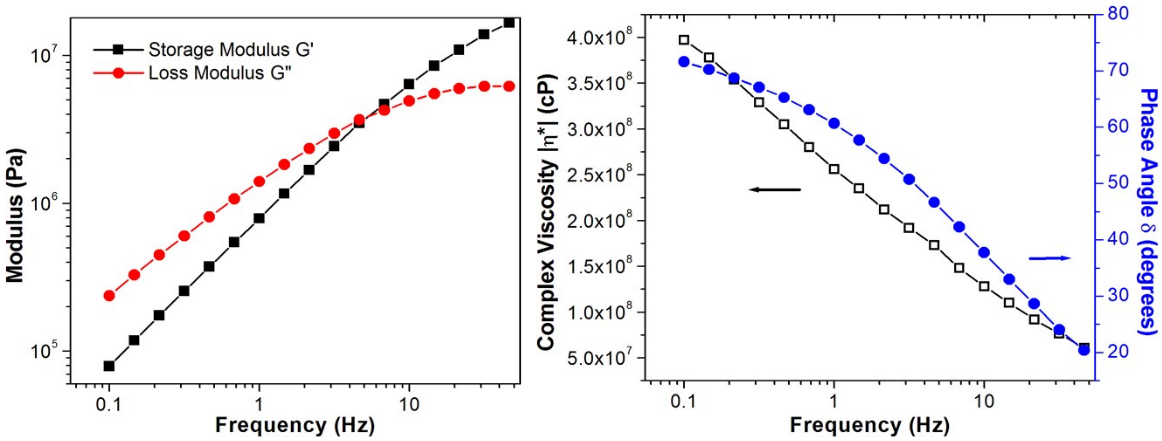

Figure S7. Oscillating rheometry data of PG 64-22 at 22 °C. The storage modulus *G'* should theoretically approach the equilibrium relaxation modulus as frequency decreases. The lowest value of G' recorded is 0.08 MPa at 0.1 Hz. The bulk bitumen is thought to be equivalent to the substrate in the "wrinkled film" hypothesis, and the applicable value of $\overline{E}_s$ should be close to the equilibrium relaxation modulus of the substrate material. Measuring $\overline{E}_f$ is not straightforward, especially not by AFM as noted in the main text. Very preliminary AFM measurements using HybriD Mode™ (NT-MDT) of the peri phase on PG 64-22 binder gave a maximum measured stiffness on the order of 1 GPa (Oleg Butyaev, Sergei Magonov, and Marko Surtchev, NT-MDT, personal communication, August – October 2015). These values would give $\overline{E}_f/\overline{E}_s \sim 10^4$ and a "bee" film thickness $h \approx 5$ nm for $\lambda_o = 450$ nm. For comparison, $\overline{E}_f/\overline{E}_s = 10^3$ gives $h = 10.3$ nm.

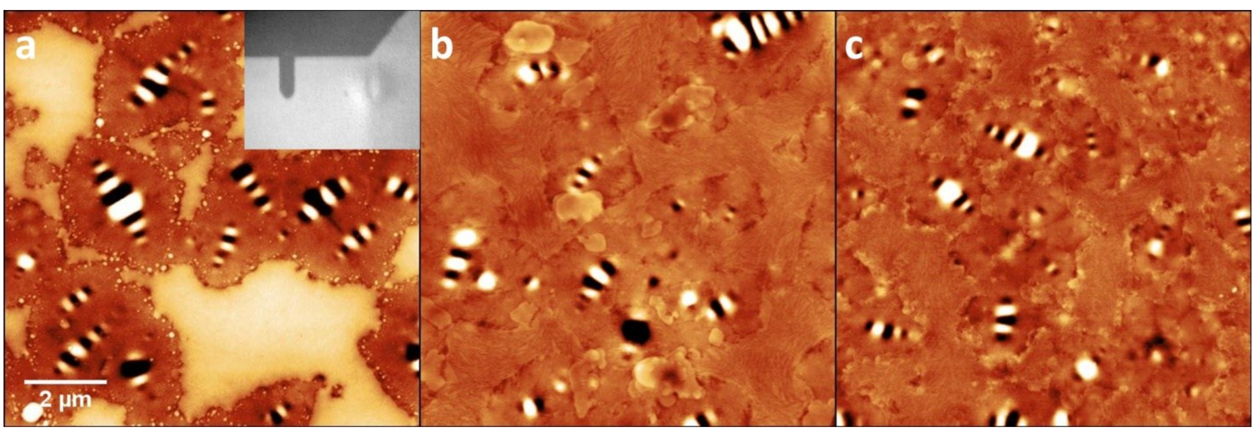

Figure S8. Topography images of the same three samples from main text Fig. 4 after 32 days of storage in (a) ambient, (b) dry, and (c) 4°C conditions, respectively, but taken at a different location 0.25 mm away. Scale bar is the same for all images. Height scale for all images is 25 nm, matching Figure 4 for comparison. A snapshot from the AFM optical camera (inset) shows a visible mark left on the sample where it was previously imaged (for scale, nominal cantilever width is 30 μm). Note that color contrast in an AFM topography image is a direct measure of height difference. The images in main text Fig. 4 look similar to these, but the features there are taller in height as evidenced by greater color contrast using the same false color height scale.